Since January 2020 Elsevier has created a COVID-19 resource centre with free information in English and Mandarin on the novel coronavirus COVID-19. The COVID-19 resource centre is hosted on Elsevier Connect, the company's public news and information website.

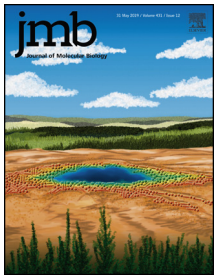

Deciphering the Nucleotide and RNA Binding Selectivity of the *Mayaro* Virus Macro Domain

Aikaterini C. Tsika [1], Efstathios Melekis [1], Sofia-Antigoni Tsatsouli [1], Nicolas Papageorgiou [2], Maria J. Maté [2], Bruno Canard [2], Bruno Coutard [3], Detlef Bentrop [4] and Georgios A. Spyroulias [1]

1 - Department of Pharmacy, *University of Patras, GR-26504 Patras, Greece*
2 - AFMB, *UMR7257 CNRS/Aix Marseille Université, Marseille, CEDEX 9, France*
3 - UVE: Aix-Marseille Univ-IRD 190-Inserm 27-IHU Méditerranée Infection, *Marseille, France*
4 - Institute of Physiology II, *Faculty of Medicine, University of Freiburg, D-79104 Freiburg, Germany*

Correspondence to Bruno Coutard and Georgios A. Spyroulias: *Bruno.Coutard@univ-amu.fr, G.A.Spyroulias@upatras.gr, http://www.bionmr.upatras.gr*
https://doi.org/10.1016/j.jmb.2019.04.013
Edited by M.F. Summers

Abstract

Mayaro virus (MAYV) is a member of *Togaviridae* family, which also includes *Chikungunya* virus as a notorious member. MAYV recently emerged in urban areas of the Americas, and this emergence emphasized the current paucity of knowledge about its replication cycle. The macro domain (MD) of MAYV belongs to the N-terminal region of its non-structural protein 3, part of the replication complex. Here, we report the first structural and dynamical characterization of a previously unexplored *Alphavirus* MD investigated through high-resolution NMR spectroscopy, along with data on its ligand selectivity and binding properties. The structural analysis of MAYV MD reveals a typical "macro" (*ββαββαβαβα*) fold for this polypeptide, while NMR-driven interaction studies provide in-depth insights into MAYV MD–ligand adducts. NMR data in concert with thermodynamics and biochemical studies provide convincing experimental evidence for preferential binding of adenosine diphosphate ribose (ADP-r) and adenine-rich RNAs to MAYV MD, thus shedding light on the structure–function relationship of a previously unexplored viral MD. The emerging differences with any other related MD are expected to enlighten distinct functions.

Introduction

Alphaviruses belong to the *Togaviridae* family, whose members form enveloped particles characterized by icosahedral symmetry enclosing their genome. They cause mainly mosquito-borne diseases in vertebrates such as birds and rodents, which act as reservoir hosts. The genus *Alphavirus* is divided in two subcategories depending on the viruses' primary areas of endemicity and clinical manifestations [1,2]. Old World *Alphaviruses* were initially identified in Asia and Africa, where they have been considered as causal agent of arthropathies [3,4]. By contrast, New World *Alphaviruses* are usually implicated in neurological diseases with complications such as dysarthria, motor disorders and abnormal reflexes, and were detected solely in the Americas [5]. *Mayaro* virus (MAYV) is an exception to this classification. Despite its endemic distribution in South America, the induced disease has a clinical picture similar to the Old World *Alphaviruses* [6]. In particular, symptoms include mild-to-severe *Dengue*-like febrile syndrome, characterized by fever, headache, rash, myalgia, arthralgia and arthritis, which can be debilitating and can persist for months [4,7,8]. These clinical manifestations are reported also in the *Chikungunya* virus (CHIKV) disease.

The resemblance of MAYV and CHIKV diseases, the worldwide outbreaks of CHIKV, and the ability of MAYV to be reproduced into mosquitoes inhabiting urban environments underline the importance of this "neglected virus" [6,9–11]. It is worth mentioning that MAYV is mainly transmitted by mosquitos of *Haemagogus* and *Aedes* genera, the latter being also responsible for the distribution of *Zika*, *Dengue* and

Chikungunya viruses. The recent *Alphavirus* outbreaks in concert with the absence of vaccines and targeted antiviral therapy emphasize the necessity to understand their replication mechanisms in detail [3,12]. The global distribution and the constantly reported outbreaks of these viral infections point out the significance of preventing the potentially chronic, disabling and long-lasting complications caused by these viruses, in order to reduce the social and economic impacts of these zoonoses.

The replication of *Alphavirus* occurs in spherules [13,14] containing four non-structural proteins (nsP1 to nsP4) [15] resulting from processing of the precursors P123 and P1234. NsP1 is carrying the enzymatic activities for the mRNA cap formation, nsP2 has a N-terminal domain with multiple enzymatic activities (e.g., ATPase, RNA helicase, RNA triphosphatase) [16–18]. Its C-terminal part is carrying a protease activity for polyprotein processing with a papain-like domain and is followed by a classical 2'*O*-methyltransferase fold [19,20]. NsP4 is carrying the RNA-dependent RNA polymerase activity [21] in charge of the replication/transcription. Many functions have been attributed to nsP3 in recent years [22]. Its C-terminal region, named HVR (hypervariable region), is a hub for interactions with several partners while its N-terminal region contains a globular macro domain (MD).

MDs are conserved and widely distributed versatile structural motifs of 130–190 amino acids. They are found both in prokaryotes and eukaryotes as well as in viruses [23–27].

Only few genera of positive-sense single-stranded RNA ((+)ss RNA) viruses contain MD folds, for example, *Alphavirus*, *Coronovirus* (CoV), *Rubella* virus and *Hepatitis E virus*. The *Alphaviruses* MDs are located at the N-terminal region of nsP3 and adopt a *β/α/β* mixed sandwich topology. Initially, MD's biological functions were linked to their ability to bind adenosine diphosphate ribose (ADP-r), its derivative (Poly-) ADP-r and RNA. In addition, *Alphaviruses* MDs were found to be adenosine di-phosphoribose 1″-phosphate phosphatases, but the role of this activity in viral replication remained elusive [27]. Subsequently, several studies proved its significance to viral replication and virulence, while recent studies proposed that the function of MDs is associated with their activity as ADP-ribosylhydrolases, suggesting their implication in counteracting responses to infection [28–36]. In general, viral MDs are postulated to be critically involved in replication complex formation, cell-specific viral replication and ADP-ribosylation dependent interactions with host proteins [37]. It remains to be investigated if and how distinct properties of different *Alphavirus*es MDs such as sequence, structure, dynamics and ligand binding can be correlated to different functions and different viral replication profiles.

ADP-ribosylation is a fundamental nucleotide-based post-translational modification that is vital to cellular processes including cell signaling, DNA repair, RNA regulation and probably many others in various organisms. The addition and the removal of an ADP-r moiety to or from cellular targets are strongly regulated processes leading to functional changes through mono-ADP-ribosylation (MARylation) and/or poly-ADP-ribosylation (PARylation). The induced alterations of enzymatic activities and the ability of ADP-ribosylated proteins to serve as "anchors" for biomolecular interactions are connected with their assigned biological roles. These include DNA damage response, transcription signaling, cellular stress response, protein degradation and immune response. Most of the aforementioned functions require the cross-talk of proteins participating in the ADP-ribosylation and in other post-translational modifications, such as ubiquitination [38–42]. Recently, it was reported that ADP-ribosylation is induced upon *Alphavirus* infection in an interferon-independent manner [37].

The enzymes and protein domains involved in ADP-ribosylation are characterized as writers, erasers and readers [42–45] based on their ability to transfer, remove and recognize ADP-r or ADP-ribosylated substrates. Among proteins binding ADP-r, MDs are classified as readers or/and erasers [42].

Herein, we address the structure–function relationship of the MAYV MD through the determination of its high-resolution NMR structure and dynamics. Furthermore, interaction studies with ADP-r, other adenosine derivatives and RNA oligonucleotides were performed through heteronuclear NMR spectroscopy, isothermal titration calorimetry (ITC) and electrophoretic mobility shift assay (EMSA) analysis. The characterization on both a structural and a biochemical level elucidates physicochemical features of the MAYV MD, reveals that non-conserved loops are crucial for the structural plasticity and substrate selectivity of the domain, and provides novel mechanistic insights into the binding of various adenosine-based ligands.

Results and Discussion

NMR solution structure of MAYV MD

The solution structure of MAYV MD was determined from more than 1600 NMR-derived geometrical restraints (PDB ID: 5IQ5; BMRB accession no. 30043) (Fig. 1a and Table S2) [46–48]. The MAYV MD, spanning residues 1335 to 1493 of P1234, is characterized by a six-stranded *β*-sheet (*β1* 4–6, *β2* 18–21, *β3* 56–60, *β4* 63–67, *β5* 103–107, *β6* 138–142) surrounded at both sides by four major *α*-helices (*α1* 34–43, *α2* 78–98, *α3* 121–134, *α4* 149–157) (Fig. 1b). The secondary structure elements are arranged in a *ββαββαβαβα* topology, with *β*3 being the only antiparallel *β*-strand. This type of folding has also been

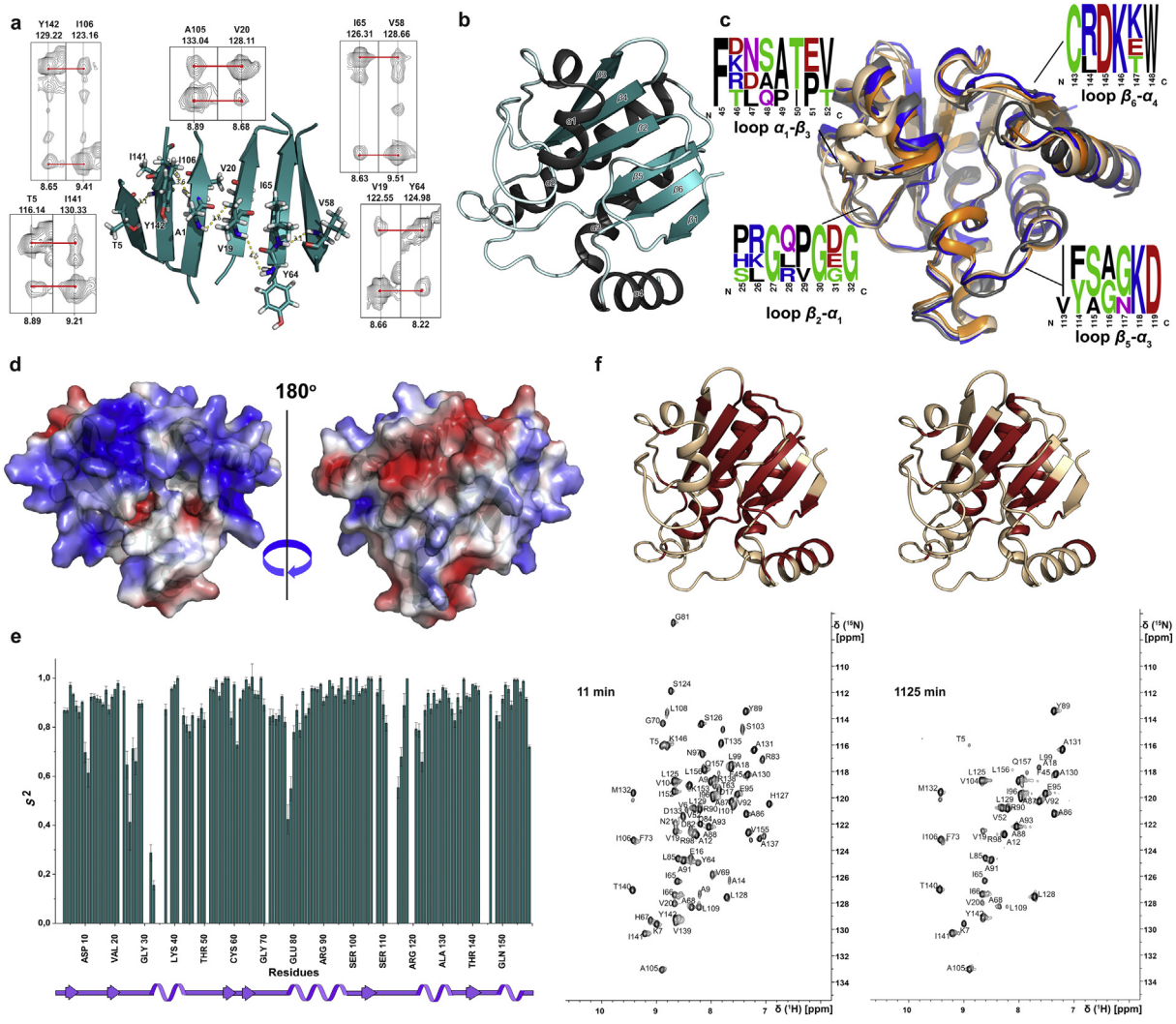

Fig. 1. (a) Characteristic NOE restraints derived from a ^{15}N-edited 3D NOESY–HSQC experiment. (b) Ribbon representation of the energy minimized average NMR model of MAYV MD. (c) Backbone superposition of MDs from MAYV (gray; PDB 5IQ5), CHIKV (orange; PDB 3GPG), SINV (blue; PDB 4GUA),and VEEV (beige; PDB 3GQE) showing also the degree of sequence conservation in four loops. (d) Representation of the electrostatic surface potential of MAYV MD (red, −4; blue, +4; calculated with the PyMol APBS extension). (e) S^2 order parameters of the backbone of MAYV MD. Residues with values close to one have a decreased mobility on the ps/ns timescale. (f) Mapping of residues with slowly exchanging backbone amide protons in the core region of MAYV MD (dark red). The corresponding ^{1}H, ^{15}N HSQC spectra at time points 11 and 1125 min of the H/D exchange experiment are shown below.

encountered in other MDs exhibiting the typical three-layered *β/α/β* sandwich topology.

As expected, its structural homologs according to DALI database [49] are the MDs of CHIKV (PDB ID: 3GPG, *Z* score: 27, RMSD: 1.3 Å), *Sindbis virus* (SINV; PDB ID: 4GUA, *Z* score: 27, RMSD: 1.4 Å), and *Venezuelan Equine Encephalitis virus* (VEEV; PDB ID: 3GQE *Z* score: 24, RMSD: 1.7 Å), all of them exhibit significant topological similarities with MAYV MD. Structural differences between these proteins are mainly localized in four loop regions (*β*2–α1, *α*1–*β*3, *β*5–*α*3, *β*6–*α*4) (Fig. 1c), which are believed to be responsible for the catalytic properties [50] and the different affinities of MDs for ADP-r [51]. A striking example is the loop *β*2–*α*1 with only two conserved glycine residues, which is considered crucial for the catalysis [50] and adopts different orientations in the four structures.

Specifically, MAYV, CHIKV and SINV MDs have at position 31 Asp or Glu instead of Gly in the VEEV sequence, while position 35 is usually occupied by charged amino acids, such as Arg (MAYV and CHIKV) or Lys (SINV), in contrast to a Gly residue in the VEEV sequence. In addition, MAYV MD has Val and Ala

at positions 29 and 38, respectively, whereas these positions are occupied by Pro and Tyr in the other three MDs.

The other three loops are important for ligand binding and exhibit ~30% sequence identity (Fig. 1c). Loop α1–β3 contains only a single conserved residue at position 45 (Phe) and exhibits different conformations in the four MDs. The only conserved residues of the loop β5–α3 are at its C-terminal end (Lys118, Asp119). The MDs of MAYV and CHIKV differ in three positions of this loop: 113 (Ile *versus* Val) 114 (Phe *versus* Tyr), and 116 (Ala *versus* Gly). Finally, the β6–α4 loop is the one with the highest number of conserved residues (four out of six residues) but plays only a minor role in ligand binding and catalysis.

Analysis of the electrostatic surface potential of MAYV MD identified a solvent accessible cleft surrounded by positively charged surface areas. Helices α1 and α4 and the loops connecting the secondary structure elements β1–β2–α1–β3 and β6–α4 contribute to the formation of this cleft that could serve as a binding site for negatively charged molecules such as RNA or (Poly-) ADP-r. The opposite side of MAYV MD is negatively charged (Fig. 1d).

Dynamic properties of MAYV MD

The dynamic properties of the polypeptide on the ps/ns timescale were derived from ^{15}N R_1 and R_2 relaxation rates and the heteronuclear $\{^1H^N\}$–^{15}N NOEs (Fig. S1) (average values of 1.53 ± 0.19 s^{-1}, 14.14 ± 2.52 s^{-1} and 0.84 ± 0.04, respectively, for residues 2–159). The correlation time for isotropic tumbling in solution as calculated from the R_2/R_1 ratio is 8.8 ns, which roughly corresponds to MW ~17.6 kDa (theoretical MW 18.1 kDa) and clearly indicates that the protein is a monomer in solution. Calculation of the S^2 order parameter (Fig. 1e) showed that the N- and C-terminal regions of MAYV MD are as rigid as most of the protein. Increased mobility on the ps/ns timescale was only found for three segments, which comprise the loops β2–α1 (Gly32-Val33), β4–α2 (Ser77-Ala79), and β5–α3 (Ser115–Gly117). Note that signals of the neighboring residues Gly30–Asp31, Cys34–Ala36, Ala38, Gly112–Phe114 and Asp119–Arg120 are broadened beyond detection in the ^1H,^{15}N heteronuclear single quantum coherence (HSQC) spectrum of the apo form of MAYV MD. Thus, their ^1H,^{15}N correlation peaks could not be assigned, strongly suggesting that the loops upstream to helices α1 and α3 undergo conformational exchange processes that may be relevant for the selectivity of substrate binding [52]. These data support the plasticity of two functionally important loops (Fig. 1c). According to our NMR data, the MAYV MD loop β2–α1 seems to be more dynamic (lower S^2 values and negative values $\{^1H^N\}$–^{15}N NOEs, while at the same region, CHIKV exhibits only positive values; data not shown) than the corresponding segment of CHIKV MD (Fig. S2). In addition, the fact that the HN resonances of the neighboring residues mentioned above (Cys34–Ala36 and Ala38) remain unidentified while the HNs of the corresponding segment in CHIKV apo MD could be assigned [53] (Fig. S2c), shows that an exchange process on an intermediate NMR timescale is present in the β2–α1 loop of MAYV MD, but not in CHIKV MD.

An H/D exchange experiment in which a ^{15}N-labeled sample was lyophilized and dissolved in 100% D_2O provided additional information on the mobility of MAYV MD on the timescale of minutes to hours. All loops, helix α1 and the outer part of helix α4 as well as the first residues of strands β1 and β3 show complete exchange of the backbone amide protons in the first 11 min of the experiment (Fig. 1f) [54]. After an exchange time of 1125 min, the HN resonances of residues that belong to the solvent-inaccessible core of the protein, which is formed by specific parts of (i) strands β2 (Ala18–Val20), β4 (Ile65–Ile66, Ala68), β5 (Val104–Ile106), and β6 (Thr139–Tyr142) and (ii) helices α2 (Leu85–Ile96), α3 (Leu128–Met132), and α4 (Leu156–Gln157), are still visible (Fig. 1f). Hence, there is a stable hydrogen bond network in this rigid core region of MAYV MD, in contrast to the mobility of the majority of residues on the min/h timescale (Fig. 1f).

MAYV MD nucleotide selectivity and binding

A series of adenosine-based molecules was used to explore the ability of MAYV MD to bind adenosine derivatives as well as to elucidate the impact of individual chemical moieties on the MAYV MD–ligand interaction and the role of certain residues in ligand recognition. Titrations of MAYV MD with ADP-r, ADP, adenosine triphosphate (ATP), adenosine monophosphate (AMP) and NAD+ were monitored by acquisition of ^1H,^{15}N HSQC spectra and showed chemical exchange between free and ligand-bound MD ranging from fast to slow on the NMR timescale.

NMR titration of the MAYV MD with ADP-r suggests a strong interaction of both molecules and complex formation at 1:1 molar ratio (Fig. 2a). Furthermore, the analysis of the backbone amide chemical shift perturbations (CSPs) identifies the residues that are involved in this process (Fig. 2c and d). To this end, a complete backbone and side-chain resonance assignment of the MAYV MD–ADP-r complex was obtained (BMRB accession no. 27612). Specifically, residues Asp10, Ala23, Asn24, Gln28, Gly32, Val33, Lys56, Val69, Ser110 and Ala116 exhibited the largest CSPs while undergoing chemical exchange between the free and the bound form in the slow exchange regime (~0.1–1 s, $k_{ex} << |\Delta\nu|$ and usually $K_d \approx$ μM or lower [52]). In addition, adjacent amino acids like Ala9, Ala12, Thr13, Gly27, Val29, Asn72, Phe73, Leu109, Ser115 and G117 were also affected exhibiting a slow-exchange process during the interaction. The backbone HN resonances of Ile11,

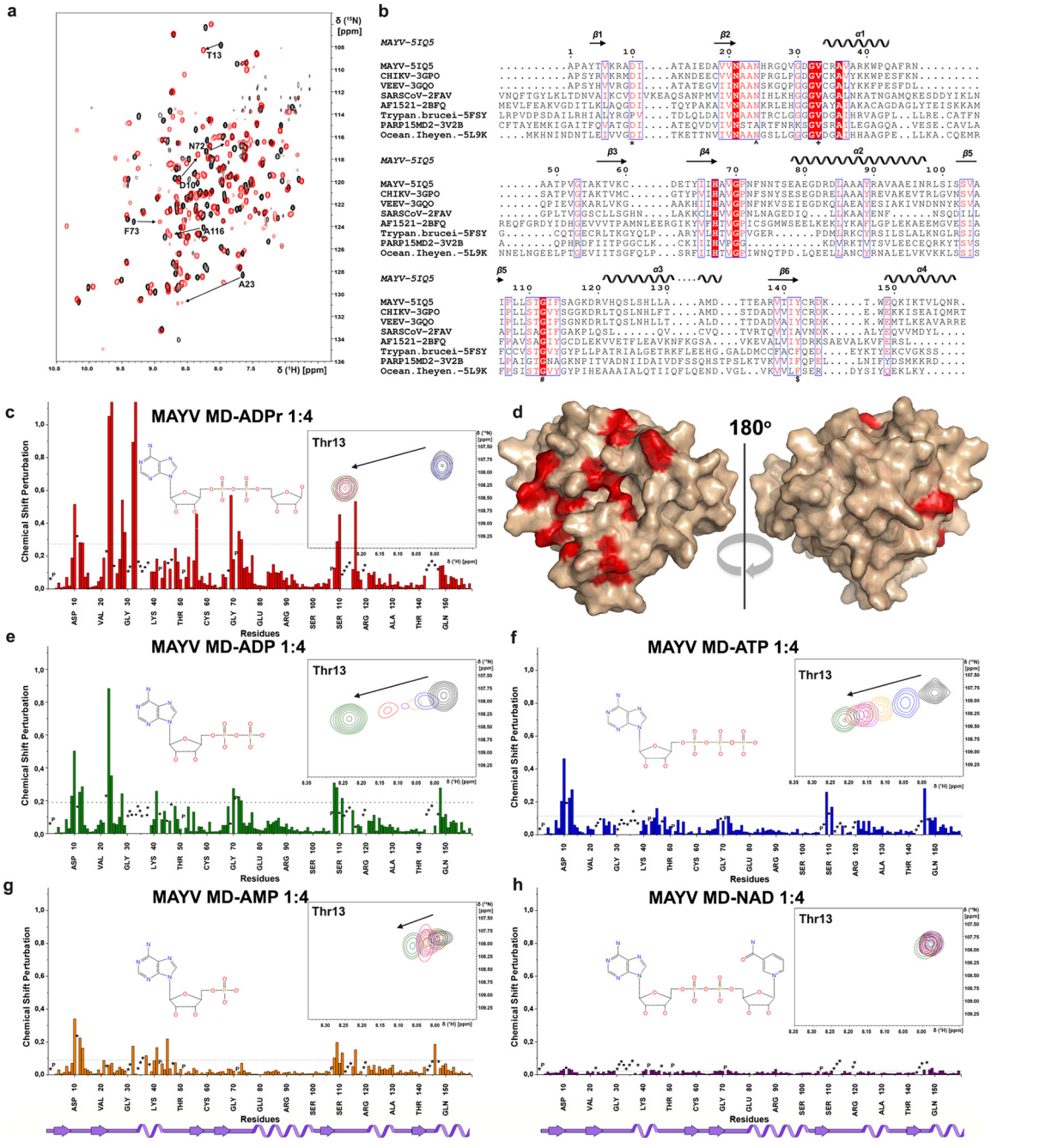

Fig. 2. (a) Superposition of the $^{1}H,^{15}N$ HSQC spectra of MAYV MD in the absence (black) and presence of ADP-r at a 1:1 molar ratio (red). Arrows indicate the changes of the peak positions of characteristic amino acids. (b) Sequence alignment of PDB-deposited MD structures in complex with ADP-r; symbols below indicate the key residues that interact with the ADP-r molecule. (c, e, f, g, h) Plots of combined amide chemical shift changes, $\Delta\delta$, induced by binding of adenine-based molecules to MAYV MD *versus* amino acid sequence at the given molar ratios of protein:ligand. In each plot, the dotted line indicates the applied threshold of chemical shift perturbation calculated as the average value plus 1 SD. An asterisk indicates an unassigned residue of apo-MD, p indicates a proline residue and a dot indicates a residue whose HN resonance could not be detected at each titration step. The $\Delta\delta$ values of Asn24 and Val33 in panel c (binding of ADP-r) are 2.2 and 3.8, respectively. Inset at right of each CSP plot: behavior of the amide peak of Thr13 during the titration indicating different binding regimes for the tested ligands (color code for the molar ratio protein:ligand: 1:0, black; 1:0.25, blue; 1:0.5, orange; 1:0.75, purple; 1:1, red; 1:3. green). (d) Surface representation of MAYV MD depicting in dark red the amino acids exhibiting CSP values above the threshold in the presence of ADP-r.

His25, Val37, Phe45, Ala68 and Lys146 broadened beyond detection, while those of Ala22, Gly30, Asp31, Cys34, Arg35, Ala36, Ala38, Gly112, Cys143 and Arg144, which were unassigned in the spectra of the apo MAYV MD, could be assigned in the $^{1}H,^{15}N$ HSQC spectrum of the MAYV MD–ADP-r complex. These data suggest that the majority of the residues, which participate in ligand recognition and binding, are located near the positively charged ligand-binding cleft (Figs. 1d and 2d). It is worth mentioning that upon binding of ADP-r, the backbone and side-chain resonances of residues in the loops that comprise the positively charged cavity are observable, while they were not detectable in the free state of the protein. All these findings prove the high-affinity interaction of MAYV MD with ADP-r and indicate ligand binding via loops $\beta1$–$\beta2$, $\beta2$–$\alpha1$, $\beta4$–$\alpha2$, and $\beta5$–$\alpha3$, which should comprise or be located nearby the anticipated binding cleft (Fig. 2d) [52]. Most residues in these loops show relatively low-order parameters (Fig. 1e) or conformational averaging in the apo state.

Then NMR data showed that the complex formation with ADP required a 1:3 (protein:ligand) molar ratio (no further chemical shift changes observed at higher ligand concentrations up to a 1:4 molar ratio) and that the exchange occurred in the intermediate time regime ($k_{ex} \sim |\Delta v|$), strongly suggesting that ADP interacts more weakly than ADP-r. Similar to ADP-r, the addition of ADP to MAYV MD induced the largest chemical shift perturbations in the loops connecting the $\beta1$ and the $\beta2$ strands (Ala9–Thr13), the $\beta2$ strand and the $\alpha1$ helix (Ala23–His25), the $\beta4$ strand and the $\alpha2$ helix (Asn72, Phe73), and the $\beta5$ strand and the $\alpha3$ helix (Leu108–Thr111) (Fig. 2e). During the titration with ADP the HN resonances of Ala9, Asp10, Ala12, Thr13 (Fig. 2e, inset), Ala23–Gly27, Val37, Gly70, Leu108, Leu109, Thr111, Ser115 and Gly117 are shifted and broadened, exhibiting intermediate-to-fast exchange, different from the slow-exchange process that they undergo during interaction with ADP-r. The HN resonances of the residues Ile11, Gly32, Val33, Val37, Val69, Ser110 and Ala116 could not be identified at the final step of the titration due to broadening of the corresponding peaks, indicating chemical exchange processes on an intermediate NMR timescale (Fig. 2e).

ATP was subsequently tested as a putative ligand for MAYV MD to explore the role of the negatively charged phosphate groups. The complex formation is achieved at a molar ratio of 1:4 (protein:ligand) and led to smaller CSP values than the intermediate or slow chemical exchange during the titrations with ADP and ADP-r, respectively. However, the residues exhibiting CSPs are practically the same as in the case of ADP. Similarly, the $^{1}H,^{15}N$ HSQC cross peaks of Ile11, Ala23, Asn24, Gly32, Val33, Val69, Leu108, Ser110 and Ala116 remained broadened beyond detection even after the last addition of ATP (Fig. 2f). On the other hand, Asp10, a key residue for the ligand binding, is in the fast-exchange regime upon addition of ATP to MAYV MD. The same behavior was observed for the other key residues Thr13 (Fig. 2f) and Leu109. Therefore, the interaction can be characterized best as fast exchange on the NMR timescale ($k_{ex} >> |\Delta v|$). Such an analysis of the binding kinetics can also provide an estimate of the binding affinity [52,55], which in this case implies a weak binding with a K_d of the order of $\sim 10^{-3}$ M. Therefore, it may be concluded that ATP binds less tightly than ADP.

Titration of MAYV MD with AMP, the simplest adenosine derivative used in this study, was characterized by relatively small CSPs and fast exchange, while the affected regions are the same as with the other ligands. (Fig. 2g). As with ATP, Asp10 in the $\beta1$–$\beta2$ loop is in fast exchange and shows a prominent chemical shift change. Note that Ala23 in the $\beta2$–$\alpha1$ loop whose HN resonance was broadened beyond detection during the ATP titration was observed up to the last stage of the titration with AMP. Moreover, the CSP of Val37 in the first turn of helix $\alpha1$ could be followed at all titration steps for the first time. Ala116 in the $\beta5$–$\alpha3$ loop showed slow exchange with ADP-r, intermediate exchange in the titrations with ADP and ATP, but fast exchange in the case of AMP. These observations exemplify the adaptability of MAYV MD to adenosine-based ligands.

Titration of MAYV MD with NAD+ up to a molar ratio of 1:4 (protein:NAD+) had only a minor influence on the $^{1}H,^{15}N$ resonances of the protein indicating that NAD+ exhibits the weakest interaction among the five nucleotides tested. The intensities of the cross peaks of Ala23, Asn24, Gly32 and Ser110 are decreased or broadened beyond detection at the final step of titration. These observations indicate that despite the weak protein–NAD+ interaction, these residues are affected more by the addition of NAD+ than by AMP. The segments influenced by NAD+ are the $\beta1$–$\beta2$ loop, the $\beta5$–$\alpha3$ linker, the C-terminal end of the $\beta6$–$\alpha4$ loop and the first $\alpha4$ residues (Fig. 2h). Although NAD+ interacts only weakly with the protein, it is the only ligand that induces CSPs above threshold (lower than the threshold of any of the other four nucleotides) for the backbone HN resonances of Gln43 and Ala44 at the C-terminus of helix $\alpha1$, suggesting a different interaction interface for the relatively bulky NAD+ (Fig. S3).

The screening of adenosine-based molecules for their potential binding to MAYV MD revealed that ADP-r exhibits the strongest interaction and forms a 1:1 complex. In addition, the role of individual chemical moieties of the ADP-r molecule can be evaluated through a comparative analysis of the ligand-induced chemical shift changes (Figs. 2 and

S3). The ligands used (ADP-r, ADP, ATP, AMP and NAD+) differ in each case in the chemical group connected to adenosine, thus allowing to elucidate the contribution of each moiety to the chemical shift changes. Absence of the terminal ribose moiety has a significant effect on the interaction, since ADP-r is the only MAYV MD ligand leading to a slow-exchange process on the NMR timescale ($k_{ex} << |\Delta\nu|$). In general, ADP and AMP interact with the same residues of MAYV MD, but interestingly, the residues that interact with the β-phosphate group of ADP can be identified clearly. According to the literature [50], there are two structural water molecules that are H-bonded to the β-phosphate. In the crystal structures of the MDs from *Oceanobacillus iheyensis* (PDB ID: 5L9K) and CHIKV (PDB ID: 3GPO) in complexes with ADP-r, these water molecules interact with the conserved residues Ala29, Gly91 and Ala23, Gly70, respectively. Ala23 and Gly70 in MAYV MD exhibit much smaller CSPs (Fig. 2g and e) and undergo a fast-exchange process upon the addition of AMP compared to ADP, indicating an active role in the binding of the second phosphate group.

AMP and especially NAD+ exhibit weak interaction. The addition of a substituted pyridine ring to the distal ribose of ADP-r seems to impede the access of NAD+ to the binding cavity of the smaller adenosine derivatives.

Identification of MAYV MD residues critical for ADP-r binding through NMR and ITC

To further characterize the MAYV MD–ADP-r interaction, MD mutants were designed considering the most affected regions in the CSP analysis (Fig. 2c) as well as available crystal structures of MD–ADP-r complexes [25,27,28,50,56,57] from various organisms. These structures reveal conserved patterns of amino acids that mediate the interaction of ADP-r with the protein (Fig. 2b). According to these models, the NH_2 group of adenine forms a hydrogen bond with the carboxyl group of an aspartate (Fig. 2b, indicated with "$_{\star}$") at the beginning of the $\beta1$–$\beta2$ loop. The hydrophobic residue (Ile/Val) following this aspartate is also hydrogen-bonded to adenine via its backbone amide group. In several homologous structures (e.g., PDB ID: 2BFQ), an aromatic residue (Tyr/Phe) (indicated with "$" in Fig. 2b) is found to stabilize further the adenine through π–π stacking to its purine ring. The phosphate groups are connected through their oxygen atoms to the backbone amides of residues in two conserved sequence motifs around almost invariable Gly residues. The first motif is a Gly followed by Val/Leu just before helix $\alpha1$ (Fig. 2b, indicated with "$_{+}$"), and the second one is Ser/Gly–X/Thr–Gly–Ile/Val/Asn–Tyr/Phe/Leu/Ala in the $\beta5$–$\alpha3$ loop (Fig. 2b, indicated with "$_{\#}$"). Finally, the distal ribose is stabilized by a hydrogen bond to an Asn residue in the $\beta2$–$\alpha1$ loop (Fig. 2b, indicated with "$_{\wedge}$") [56–59]. These residues, namely, Asp10/Ile11, Gly32/Val33, Gly112 and Asn24, are also present in MAYV MD (Fig. 2b) and interact with ADP-r as clearly shown by our CSP data (Fig. 2c and Fig. S3a).

Surprisingly, the weakly conserved residues Asn72 and Phe73, in the $\beta4$–$\alpha2$ loop, are also strongly affected by the binding of ADP-r indicating a rearrangement of this loop.

The impact of residues Asp10, Asn24 and Phe114 on the binding of ADP-r to MAYV MD was examined by means of three mutants: D10A, N24A/F114A and the triple mutant D10A/N24A/F114A. Titrations of all mutants with ADP-r were followed by the acquisition of ^{1}H, ^{15}N HSQC spectra (Fig. 3a). The comparison of the number of shifted backbone amide signals qualitatively showed that all mutants bind ADP-r more weakly than WT (with the triple mutant losing completely the ability to bind ADP-r), strongly supporting the implication of the three mutated residues in the interaction.

Then, the ADP-r binding properties of three MAYV MD variants were quantified using ITC (Fig. 3b). For MAYV MD WT, the results confirm a 1:1 stoichiometry. The obtained dissociation constant K_d is 10.9 ± 0.7 μM, while the NMR titration data show a slow-exchange process between free and ADP-r-bound MD. Thus, the slow exchange on the NMR timescale coincides with a relatively strong binding event (Fig. 2c). The binding is enthalpically favored ($\Delta H = -3993 \pm 68.55$ cal/mol, $\Delta S = 9.09$ cal/mol/K) indicating the formation of a complex through hydrogen bonds and hydrophobic interactions. The K_d for the N24A/F114A mutant is 52.1 ± 3.8 μM ($\Delta H = -2853 \pm 123.4$ cal/mol, $\Delta S = 9.86$ cal/mol/K). In the case of the D10A mutant and ADP-r, the titration curve could not be fitted by a binding isotherm and no K_d value was obtained. This fact emphasizes the key role of the conserved residue Asp10 for ADP-r recognition and binding (Fig. 3b).

Interaction of MAYV MD with RNA oligonucleotides

To gain insights into the RNA binding properties of MAYV MD, NMR titration studies and CSP analyses (Fig. 4a, b, c, d and e) were performed to probe the interaction of ^{15}N-labeled MAYV MD with the following RNA substrates: (1) an artificial poly-A tail mimicking natural mRNA (N_9A_{15}, a 24mer with the sequence 5'CUCCGCCCCA$_{15}$3') and (2) 12mers of adenine (A_{12}), cytosine (C_{12}), guanine (G_{12}) and uracil (U_{12}) to investigate the specificity of RNA base recognition. Each titration was conducted up to a 1:1 molar ratio of protein:RNA oligonucleotide.

The CSP analyses were carried out for four out of five tested RNA oligonucleotides. There were no clear results for the NMR titration with the G_{12} oligonucleotide due to the intensity loss of all HN resonances at the final step of the titration and precipitation of the

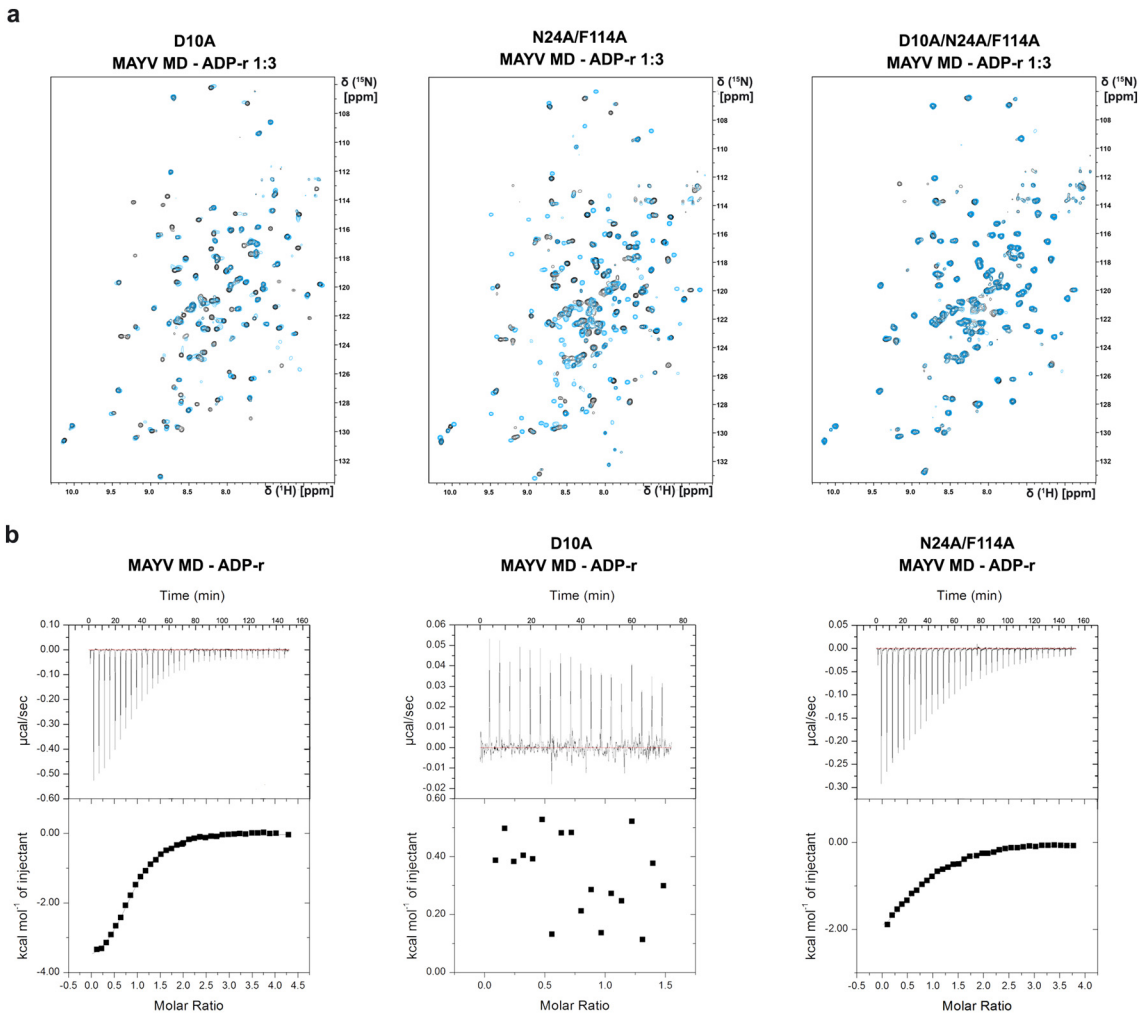

Fig. 3. (a) Superposition of the $^{1}H,^{15}N$ HSQC spectra of MAYV MD mutants (D10A, N24A/F114A, D10A/N24A/F114A) in the absence (black) and presence of ADP-r at a 1:3 molar ratio (cyan). (b) ITC data demonstrating the binding of ADP-r to MAYV MD (WT and mutants D10A and N24A/F114A). The corresponding K_d values were 10.9 µM for WT and 52.1 µM for N24A/F114A. For the D10A mutant, a K_d value could not be calculated.

sample. However, it should be noted that the first affected signals, at a MAYV MD:G_{12} ratio of 1:0.25, correspond to amino acids located at the periphery of the ADP-r binding pocket (His25–Glu28, Lys40–Trp41, Glu43, Val52, Asn97, Ser110, Gly117, Arg138, Lys146, Gln157). Denaturing PAGE analysis (data not shown) revealed that the precipitate consisted of both protein and RNA. Similar observations have been reported for SUD-M and SUD-MC domains of SARS-CoV, which have also an MD fold [60].

The NMR data showed that the addition of the four RNA oligonucleotides affects the same regions of the polypeptide. In particular the largest CSPs were observed for amino acids in or at the periphery of the positively charged ligand-binding cavity. It is worth mentioning that the presence of the RNA ligands affects residues in this binding cleft, but not in other surface areas of the MD molecule, suggesting specificity of the interaction, which is most likely driven by electrostatic attraction between positively charged surface residues of MD and negative charges of the RNA phosphate groups (Figs. 4a–d and S4).

The interactions between MAYV MD and A_{12} and N_9A_{15} influence more amino acids (14 residues with CSPs above threshold and 10 HNs broadened beyond detection for A_{12}; 17 residues with CSPs above threshold and 10 HNs broadened for N_9A_{15}) compared to U_{12} (9 CSPs above threshold and 2 HNs broadened) and C_{12} (10 CSPs above threshold and 8 HNs broadened. In agreement with literature data [27], this finding strongly suggests that MD exhibits higher affinity to the adenine oligonucleotides (N_9A_{15} and A_{12}) than to U_{12} and C_{12}. Note that the latter oligonucleotides also influence MAYV MD residues in the two loops that

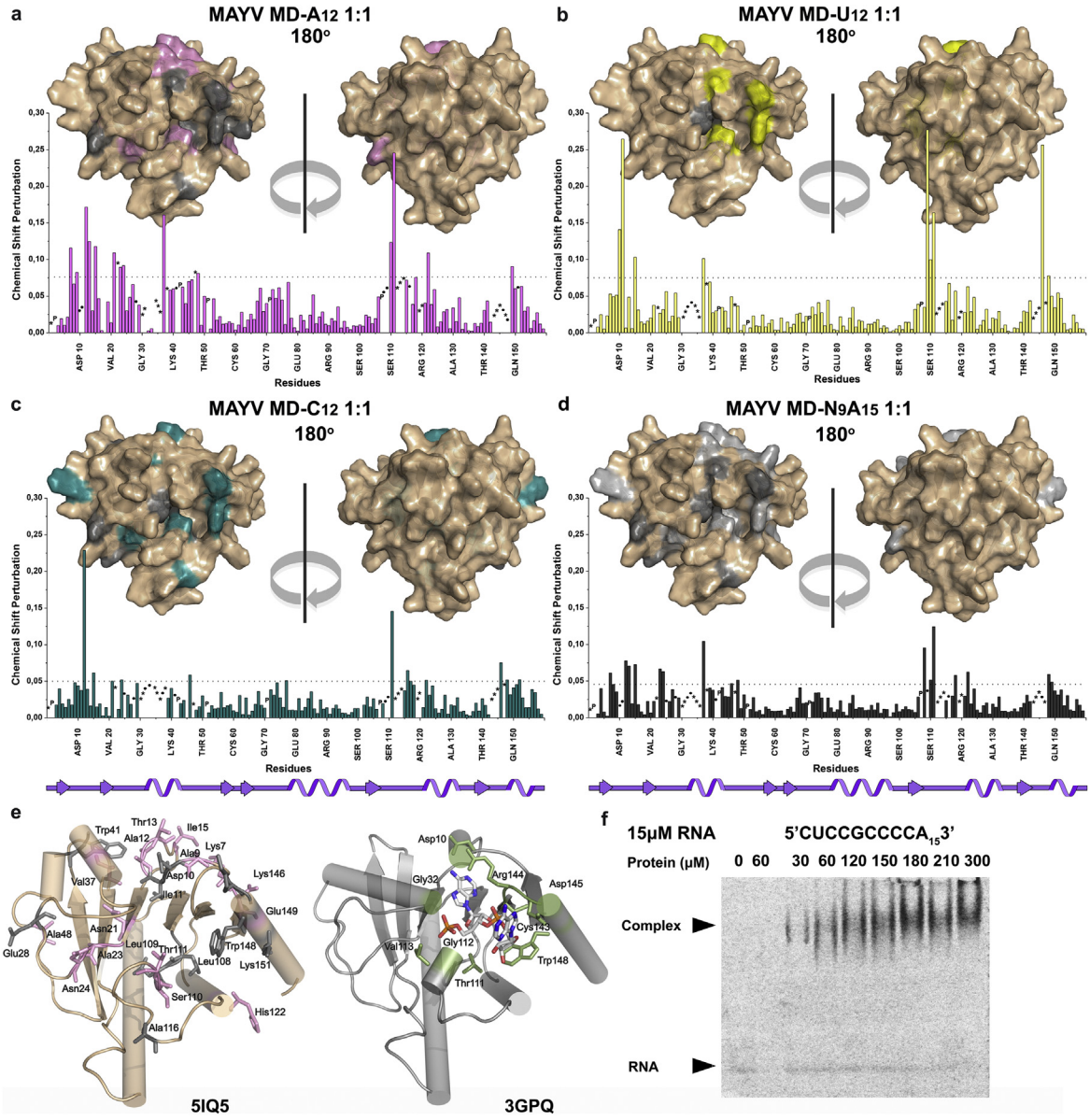

Fig. 4. (a–d) Plots of combined amide chemical shift changes, Δδ, induced by the binding of RNA oligos to MAYV MD *versus* amino acid sequence at a 1:1 molar ratio of protein:RNA oligo (pink-A_{12}, light yellow-U_{12}, dark cyan-C_{12}, gray-N_9A_{15}). In each plot, the dotted line indicates the applied threshold of chemical shift perturbation calculated as average value plus 1 SD. The surface representations above each plot show the amino acids exhibiting CSP values above the threshold upon binding of the respective RNA oligo to MAYV MD (color code: pink, A_{12}; light yellow, U_{12}; dark cyan, C_{12}; gray, N_9A_{15}) and those with broadened amide cross peaks (in dark gray). An asterisk indicates an unassigned residue of apo-MD, p indicates a proline residue and a dot indicates a residue whose HN resonance could not be detected at each titration step. (e) Left: The amino acids of MAYV MD that are critical for binding of the A_{12} oligo were mapped on its solution structure using only the amino acids with CSPs above the threshold (shown as pink sticks) and those, whose signals broadened beyond detection during the titration (in gray). Right: Representation of the residues (green sticks) that bind the A_3 molecule in the CHIKV MD-A_3 complex (PDB 3GPQ). (f) Gel shift assay (EMSA) probing the interaction of MAYV MD with the 24mer 5'CUCCGCCCCA$_{15}$3' (=N_9A_{15}). The protein concentrations used are indicated above the gel.

seem to surround the negatively charged phosphate groups in the case of ADP-r binding (β2–α1 and β5–α3) [25,27,28,50,56,57].

The MD binding surface of A_{12} is mainly defined by connecting loops and parts of helices α1 and α4. Specifically, the interaction surface is formed by the

β1–β2 loop (Lys7, Asp10, Ile11, Ala12, Thr13, Ile15), residue Ala23 in the β2–α1 loop, the amino acids Val37 and Trp41 in the α1-helix, Ala48 in the α1–β3 loop, the residues Leu109, Ser110, Ile111, Ala116, Lys118 in the β5–α3 linker and the amino acids just before and at the beginning of helix α4 (Lys146, Trp148, Glu149). The same areas are affected by N_9A_{15}.

A comparison of the interaction data of A_{12} with the crystal structure of CHIKV MD (PDB ID: 3GPQ) [27] in complex with an A_3 RNA oligonucleotide reveals that in both cases the same protein regions participate in the interaction (Fig. 4e). The higher number of amino acids that are influenced in the MAYV MD is due to the bigger size of the RNA oligonucleotide used here.

Complementary to the NMR titrations, EMSAs were conducted to verify the above-mentioned results. Three out of five single-strand RNA oligonucleotides, namely, N_9A_{15} (5'CUCCGCCCCA$_{15}$3'), A_{12} and G_{12} were tested. Since MAYV MD does not enter the polyacrylamide gel under the tested condition (theoretical pI: 9.1), the EMSA results were evaluated in terms of the complex detection. The experiments showed that there is a concentration-dependent complex formation of MAYV MD with N_9A_{15} (Fig. 4f). Moreover, binding was observed for A_{12} and G_{12} (Fig. S6).

To characterize further the selectivity of MAYV MD for nucleotides, we monitored titrations of the protein with GDP, CDP and UDP through ^{1}H,^{15}N HSQC spectra (CSP plots in Fig. S5). While the addition of CDP and UDP barely causes shifts to the ^{1}H,^{15}N resonances of MAYV MD suggesting that there is no interaction, GDP is apparently bound weakly. The interaction with GDP occurs in the fast-exchange regime, and there are only five residues with significant chemical shift changes: Ile11, Gly32, Leu109, Tyr142, and Lys146 (Fig. S5b). Compared to ADP binding (Fig. S5a), the CSPs are much smaller, no resonances are broadened beyond detection, there are no meaningful CSPs for residues Ala23–Asn24 and Val69–Asn72, and the key residue Asp10 is only minimally involved in the interaction. According to the available x-ray models [25,50] in the presence of ADP, the carboxyl group of Asp10 of MAYV MD is most likely hydrogen-bonded to the NH_2 group of adenine. However, if the orientation of the two nucleotides in the MAYV MD binding cleft were the same, this carboxyl group would repel the carbonyl oxygen on the C6 atom of guanine, which may explain the weaker interaction of GDP observed here. On the other hand, Ile11 usually forms a hydrogen bond to the base moiety of ADP and is still found to interact with GDP.

The data presented here indicate that both nucleotides and RNA oligonucleotides interact with MAYV MD. Our NMR data clearly identify the MD surface region involved in these biomolecular interactions. Adenine-rich RNA and ADP-r make use of the same binding cleft to dock onto the protein, but in the case of RNA binding, the α4 helix is additionally involved in the interactions. The observed interactions of MAYV MD with C_{12} and U_{12} RNA oligonucleotides are driven putatively by electrostatic attraction. This hypothesis is based on the absence of interaction between CDP or UDP and MAYV MD (Fig. S5c and d). The oligonucleotides C_{12} and U_{12} seem to bind to the positively charged cleft of the protein (Fig. 4b and c) due to their increased negative charge compared to the diphosphate nucleotides.

Concluding Remarks

Overall, this work reports the first solution structure of MAYV MD and identifies the protein residues involved in selective binding of ADP-r and adenine-containing ssRNA oligonucleotides to MAYV MD. This selectivity characterizes a number of MDs, and data reported herein show that MAYV MD shares structural and functional features with other *Alphavirus* MDs. The MAYV MD polypeptide folds into a well-ordered structure in solution, characterized by the β/α/β "sandwich" topology and peptide segments with functionally relevant intrinsic flexibility. These segments surround a well-defined binding pocket, which provides high selectivity and variable affinity toward adenosine derivatives and adenine-rich RNA oligonucleotides, with a preference for ADP-r. The critical role [27] of Asp10 for ligand binding is confirmed by a dramatic reduction of binding affinity upon its mutation to Ala. Moreover, this study demonstrates that non-conserved residues in loop regions, like β2–α1, α1–β3 and β5–α3, induce different local conformations and backbone dynamics in MAYV MD compared to other homologous MDs, thus customizing its ligand binding properties. This finding may represent a general principle in the structure–function relationship of viral MDs and precludes the prediction of ligand interactions and function on the sole basis of sequence homology [30,51]. Note that ADP-r binding has recently been correlated in different cell lines with immediate or slow viral replication [42].

According to the literature, there are striking examples of highly homologous MDs with distinct function, such as those from (a) CHIKV and *Semliki Forest* virus (SFV) and (b) group 1 and group 3 CoV. In the former case, the two MDs have ~77% sequence identity, but SFV does not bind ADP-r [30]. In the latter case, a group 3 CoV MD exhibits great structural similarity to a group 1 CoV MD, but does not bind ADP-r, whereas the group 1 CoV MD binds ADP-r with a K_d in the μM range [61,62]. A similar finding has also been reported for MDs of the *Alphavirus* family. Some of us have observed different binding properties for the two MDs from VEEV and CHIKV, when they attempted to form the a MD–ADP-r complex [27]. VEEV MD, which has 59% sequence identity with

CHIKV MD, did not bind ADP-r due to an unfavorable reorientation of the N24 and F114 side chains, when VEEV crystals were soaked with ADP-r. This finding suggests that even minor conformational differences in the loops β2–α1 and β5–α3 (Fig. 1c) can fine-tune the substrate binding capacity of closely related MDs. The differences in structure and mobility of the MAYV MD loops β2–α1, α1–β3 and β5–α3 with respect to CHIKV (Figs. 1c, S1 and S2) provide new insights into the structural basis of the functional role of these MD polypeptide segments. In addition, the structure elucidation of the MAYV MD along with the NMR driven interaction studies between the MD and ssRNA defines the positively charged surface illustrated in Fig. 1d, which represents another binding site, distinct from the ADP-r binding crevice, and its role in binding negatively charged biopolymer(s) (Fig. 4). These results are in line with the different roles of MD during the early and late stages of viral replication, in which a multi-functional domain is likely required [37]. The observations presented here enlighten the structural and physicochemical determinants of MD-ligand interactions and provide valuable functional insights into the MD of this neglected virus reinforcing the efforts to design novel structure-based inhibitors of this *Alphavirus* protein domain.

Methods

Expression and purification of MAYV MD and its variants

The construction of the recombinant vector containing the gene of MAYV MD, the purification procedure of the protein and the preparation of the labeled samples are described elsewhere [46]. The TRVL 4675 strain used in this study has a Thr at position 5 of the polypeptide sequence (GenBank MK070492.1).

In order to obtain high purity for the binding assays, a size exclusion chromatography was added using a Superose 12 10/300 GL column (GE Healthcare) on an Äkta Purifier system (GE Healthcare) with 10 mM HEPES, (pH 7.0) and 20 mM NaCl as elution buffer.

The fractions containing MAYV MD were pooled and concentrated to a final volume of 500 µL. The solution was then supplemented with 50 µL of D_2O and DTT was added to a final concentration of 1–2 mM. The protein concentration in the NMR samples that were used for the titrations varied from 0.1 to 0.6 mM.

The MAYV MD mutants (D10A, N24A/F114A; D10A/N24A/F114A) were obtained by PCR mutagenesis reaction using the plasmid containing the MAYV MD native gene as template and primers carrying the appropriate mutated codons. The expression and purification of the mutants were done according to the protocol for the native form of the protein.

Structure determination

All NMR experiments were recorded at 298 K on a Bruker Avance 600-MHz NMR spectrometer, equipped with a cryogenically cooled pulsed-field gradient triple-resonance probe (TXI), and on a Bruker Avance III High-Definition four-channel 700-MHz NMR spectrometer equipped with a cryogenically cooled 5 mm $^{1}H/^{13}C/^{15}N/D$ Z-gradient probe (TCI) (acquisition parameters in Table S1). All chemical shifts were referenced to internal 2,2-dimethyl-2-silapentane-5-sulfonic acid (DSS) [46].

The NMR data were processed with the TOPSPIN 3.3 software and analyzed with XEASY [63] and CARA [64]. Distance constraints for structure determination were obtained from ^{15}N- and ^{13}C-edited 3D nuclear Overhauser effect spectroscopy (NOESY)–HSQC experiments and ^{1}H–^{1}H 2D NOESY spectra, all recorded on the 700-MHz NMR spectrometer. Eighty-four torsion angle constraints used in the structural calculations were derived from TALOS+ [65]. Structure calculations were then performed through iterative cycles of DYANA [47], followed by restrained energy minimization with AMBER [48] applied to each member of the final family of 20 DYANA models and the average model.

The NMR solution structure is characterized by a target function tf = 0.73 ± 7.87 × 10^{-2} Å^2 and RMSD values of 1.07 ± 0.14 and 1.84 ± 0.14 Å for backbone and heavy atoms, respectively (Table S2). The coordinates of the energy-refined models (21 models, including the energy minimized average model) along with the structural constraints were deposited in the RCSB Protein Data Bank (PDB ID: 5IQ5). A small number of backbone and side-chain dihedral angles exhibit non-favorable values due to minor gaps in the assignment and missing experimental data.

All figures showing structures were generated using PyMol [66].

^{15}N-relaxation studies

Relaxation experiments (^{15}N $T1$, $T2$ and $\{^{1}H^{N}\}$–^{15}N NOE) were conducted using the aforementioned spectrometers at 298 K. The delays for the ^{15}N $T1$ were 7, 18, 40, 85, 150, 230, 350, 500, 680 and 900 ms, while delays of 16.99, 33.98, 50.98, 67.97, 84.96, 101.95, 135.94, 186.91 and 220.9 ms were used in the ^{15}N $T2$ experiments. The model-free approach in the TENSOR CEA/CNRS60 program was used in order to obtain the S^2 values. The S^2 values of MAYV MD are presented in Fig. 1e, while comparison of the S^2 values of the MDs from CHIKV and MAYV is shown in Fig. S2.

A H/D exchange experiment was performed with MAYV MD by dissolving a lyophilized sample of fully protonated uniformly ^{15}N-labeled protein in 100% D_2O and recording a series of ^{1}H, ^{15}N HSQC spectra

at 298 K on the 600-MHz NMR spectrometer. Each HSQC spectrum lasted 14 min 40 s, and the midpoint of acquisition of the first spectrum was 11 min after dissolution of the sample in D_2O.

NMR binding studies of ADP-r, nucleotides and RNA

The interactions of MAYV MD with adenosine-based ligands, GDP, CDP, UDP and ss RNAs were evaluated by comparing the 2D $^{1}H,^{15}N$ HSQC spectra in the presence and absence of each tested molecule. The titrations were incremental and a $^{1}H,^{15}N$ HSQC spectrum was recorded after each addition. The titrations were stopped when no further spectral changes were observed. Combined amide chemical shift perturbations were calculated using the equation: $\Delta\delta = [(\Delta\delta_{HN})^2 + (\Delta\delta_N/5)^2]^{1/2}$ [67]. In order to apply a consensus approach for the identification of shifts that are large enough to be considered as indicators of the binding site in more than 10 interaction studies between MAYV MD and small molecules or RNA oligos, we always applied the widely used method to calculate a threshold value [68–71]. This threshold is based on the calculation of the average CSP value and the SD σ and sets an unbiased criterion to detect the residues that are significantly involved in an interaction.

ITC

ITC measurements were performed at 293 K using a MicroCal ITC200 instrument (Malvern). Experiments were conducted in a buffer containing 25 mM HEPES (pH 7.5) and 150 mM NaCl. The protein concentration in the cell was between 80 μM (*wt* protein) and 120 μM (mutant protein), whereas the ADP-r concentration in the syringe was 600 to 800 μM. Heats of dilution were measured by injecting the ligand into the protein solution. Titration curves were fitted with the MicroCal Origin software, assuming a one-site binding model, and enthalpy (ΔH), entropy changes (ΔS), dissociation equilibrium constants (K_d) and stoichiometry were extracted.

EMSAs

Purified MAYV MD was incubated with ssRNA oligomers in reaction buffer containing 20 mM Tris base (pH 7), 100 mM KCl, 3 mM $MgCl_2$, 0.5 mM EDTA and 1 mM DTT in DEPC H_2O. The protein–nucleic acid mixtures were incubated at 37 °C for 15 min, followed by 30-min incubation at 25 °C. Then 6% glycerol was added, and the mixtures remained on ice for at least 15 min. The reactions were analyzed on 6% non-denaturing PAGE in the presence of 3 mM Tris-borate buffer (pH 8) at 80 V for 1 h at 4 °C.

Nucleic acid was detected by GelRed (Biotium) staining and visualized using a UV light source equipped with a digital camera. GelRed was washed out and protein was subsequently detected by Coomasie staining (Bio-Rad).

The concentration of each ssRNA transcript was 15 μM. MAYV MD was used in increasing concentrations of 30, 60, 120, 150, 180, 210 and 300 μM.

MAYV MD does not enter the polyacrylamide gel under the conditions used here due to its basic pI (calculated pI = 9.1). Therefore, it could not be detected by PAGE analysis. However, its complexes with RNA carry enough negative charge to enter the gel and to be observed as discrete bands.

Accession numbers

The backbone assignments of the MAYV MD have been deposited to the BMRB (Biological Magnetic Resonance Data Bank) under accession numbers 30043 (apo form of the protein) and 27612 (protein with ADP-r complex), while the 3D structural models have been deposited in the Protein Data Bank (ID 5IQ5).

Acknowledgments

We thank Prof. C. Stathopoulos and Dr. M. Apostolidi (Department of Medicine, University of Patras) for useful discussions and their support and help with EMSA, and Dr. B. Fakler (University of Freiburg) for continued support. EU FP7 REGPOT CT-2011-285950—"SEE-DRUG" project is acknowledged for financial support (D.B., G.A.S.) as well as for the purchase of UPAT's 700-MHz NMR equipment. The research work was supported by the Hellenic Foundation for Research and Innovation and the Greek General Secretariat for Research and Technology HFRI for a PhD Fellowship grant (A.C.T.; GA. no. 2430) and European program H2020 under the EVAg Research Infrastructure (grant agreement No. 653316). We also acknowledge partial support of this work by the project *"INSPIRED - The National Research Infrastructures on Integrated Structural Biology, Drug Screening Efforts and Drug target functional characterization"* (MIS 5002550), which is implemented under the Action "Reinforcement of the Research and Innovation Infrastructure", funded by the Operational Programme "Competitiveness, Entrepreneurship and Innovation" (NSRF 2014-2020) and co-financed by Greece and the European Union (European Regional Development Fund).

Appendix A. Supplementary data

Supplementary data to this article can be found online at https://doi.org/10.1016/j.jmb.2019.04.013.

Received 30 November 2018;
Received in revised form 1 March 2019;
Accepted 8 April 2019
Available online 16 April 2019

Keywords:
Mayaro virus;
Alphavirus;
macro domain;
ADP-ribose;
RNA

Abbreviations used:
MAYV, *Mayaro* virus; CHIKV, *Chikungunya* virus; VEEV, *Venezuelan Equine Encephalitis* virus; SINV, *Sindbis* virus; MD, macro domain; ss(+) RNA, positive-sense single-stranded RNA; ADP-r, adenosine diphosphate ribose; ADP, adenosine diphosphate; ATP, adenosine triphosphate; AMP, adenosine monophosphate; NAD, nicotinamide adenine dinucleotide; HSQC, heteronuclear single quantum coherence; NOESY, nuclear Overhauser effect spectroscopy; CSP, chemical shift perturbation; ITC, isothermal titration calorimetry; EMSA, electrophoretic mobility shift assay.

References

[1] E.G. Strauss, J.H. Strauss, Viruses and Human Disease, Academic Press, 2007.
[2] C.M. Fauquet, M.A. Mayo, J. Maniloff, U. Desselberger, L.A. Ball, Virus Taxonomy, VIIIth Report of the International Committee on Taxonomy of Viruses, Elsevier/Academic Press, London, 2005.
[3] K.D. Ryman, W.B. Klimstra, Host responses to alphavirus infection, Immunol. Rev. 225 (2008) 27–45.
[4] O. Schwartz, M.L. Albert, Biology and pathogenesis of Chikungunya virus, Nat. Rev. Microbiol. 8 (2010) 491–500.
[5] N. Forrester, G. Palacios, R. Tesh, N. Savji, H. Guzman, M. Sherman, S. Weaver, W. Lipkin, Genome-scale phylogeny of the alphavirus genus suggests a marine origin, J. Virol. 86 (2012) 2729–2738.
[6] R.B. Tesh, D.M. Watts, K.L. Russell, C. Damodaran, C. Calampa, C. Cabezas, G. Ramirez, B. Vasquez, C.G. Hayes, C.A. Rossi, Mayaro virus disease: an emerging mosquito-borne zoonosis in tropical South America, Clin. Infect. Dis. 28 (1999) 67–73.
[7] A.J. Rodríguez-Morales, A.E. Paniz-Mondolfi, W.E. Villamil-Gómez, J.C. Navarro, Mayaro, Oropouche and Venezuelan equine encephalitis viruses: following in the footsteps of Zika? Travel Med. Infect. Dis. 15 (2017) 72–73.
[8] F.W. Santiago, E.S. Halsey, C. Siles, S. Vilcarromero, C. Guevara, J.A. Silvas, C. Ramal, J.S. Ampuero, P.V. Aguilar, Long-term arthralgia after Mayaro virus infection correlates with sustained pro-inflammatory cytokine response, PLoS Negl. Trop. Dis. 9 (2015), e0004104.
[9] P.F. Vasconcelos, C.H. Calisher, Emergence of human arboviral diseases in the Americas, 2000–2016, Vector Borne Zoonotic Dis. 16 (2016) 295–301.
[10] I.M. Mackay, K.E. Arden, Mayaro virus: a forest virus primed for a trip to the city? Microbes Infect. 18 (2016) 724–734.
[11] O. Lwande, V. Obanda, G. Bucht, G. Mosomtai, V. Otieno, C. Ahlm, Global emergence of alphaviruses that cause arthritis in humans, Infect. Ecol. Epidemiol. 5 (2015), 29853.
[12] M.G. Cavalheiro, L.S.D. Costa, H.S. Campos, L.S. Alves, I. Assuncão-Miranda, A.T. Poian, Macrophages as target cells for Mayaro virus infection: involvement of reactive oxygen species in the inflammatory response during virus replication, An. Acad. Bras. Cienc. 88 (2016) 1485–1499.
[13] L. Kääriäinen, T. Ahola, Functions of alphavirus nonstructural proteins in RNA replication, Prog. Nucleic Acid Res. Mol. Biol, vol. 71, Academic Press, Cambridge, MA 2002, pp. 187–222.
[14] M.K. Pietilä, M.J. van Hemert, T. Ahola, Purification of highly active alphavirus replication complexes demonstrates altered fractionation of multiple cellular membranes, J. Virol. 92 (2018) e01852-17.
[15] K. Hellström, K. Kallio, A. Utt, T. Quirin, E. Jokitalo, A. Merits, T. Ahola, Partially uncleaved alphavirus replicase forms spherule structures in the presence and absence of RNA template, J. Virol. 91 (2017) e00787-17.
[16] Y.A. Karpe, P.P. Aher, K.S. Lole, NTPase and 5′-RNA triphosphatase activities of Chikungunya virus nsP2 protein, PLoS One 6 (2011), e22336.
[17] P.K. Das, A. Merits, A. Lulla, Functional cross-talk between distant domains of Chikungunya virus non-structural protein 2 is decisive for its RNA-modulating activity, J. Biol. Chem. 289 (2014) 5635–5653.
[18] I. Das, I. Basantray, P. Mamidi, T.K. Nayak, B. Pratheek, S. Chattopadhyay, S. Chattopadhyay, Heat shock protein 90 positively regulates Chikungunya virus replication by stabilizing viral non-structural protein nsP2 during infection, PLoS One 9 (2014), e100531.
[19] A.T. Russo, M.A. White, S.J. Watowich, The crystal structure of the Venezuelan equine encephalitis alphavirus nsP2 protease, Structure 14 (2006) 1449–1458.
[20] A. Golubtsov, L. Kääriäinen, J. Caldentey, Characterization of the cysteine protease domain of Semliki Forest virus replicase protein nsP2 by in vitro mutagenesis, FEBS Lett. 580 (2006) 1502–1508.
[21] M.W. Chen, Y.B. Tan, J. Zheng, Y. Zhao, B.T. Lim, T. Cornvik, J. Lescar, L.F.P. Ng, D. Luo, Chikungunya virus nsP4 RNA-dependent RNA polymerase core domain displays detergent-sensitive primer extension and terminal adenylyltransferase activities, Antivir. Res. 143 (2017) 38–47.
[22] B. Götte, L. Liu, G.M. McInerney, The enigmatic alphavirus non-structural protein 3 (nsP3) revealing its secrets at last, Viruses 10 (2018) 105.
[23] K.L. Feijs, A.H. Forst, P. Verheugd, B. Lüscher, Macrodomain-containing proteins: regulating new intracellular functions of mono (ADP-ribosyl) ation, Nat. Rev. Mol. Cell Biol. 14 (2013) 443–451.
[24] W. Han, X. Li, X. Fu, The macro domain protein family: structure, functions, and their potential therapeutic implications, Mutat. Res. Rev. Mutat. Res. 727 (2011) 86–103.
[25] G.I. Karras, G. Kustatscher, H.R. Buhecha, M.D. Allen, C. Pugieux, F. Sait, M. Bycroft, A.G. Ladurner, The macro domain is an ADP-ribose binding module, EMBO J. 24 (2005) 1911–1920.
[26] L. Aravind, D. Zhang, R.F. de Souza, S. Anand, L.M. Iyer, The natural history of ADP-ribosyltransferases and the ADP-ribosylation system, in: F. Koch-Nolte (Ed.) Endogenous ADP-Ribosylation, vol. 384, Springer International Publishing, Cham 2015, pp. 3–32.
[27] H. Malet, B. Coutard, S. Jamal, H. Dutartre, N. Papageorgiou, M. Neuvonen, T. Ahola, N. Forrester, E.A. Gould, D. Lafitte, The crystal structures of Chikungunya and Venezuelan equine encephalitis virus nsP3 macro domains define a conserved adenosine binding pocket, J. Virol. 83 (2009) 6534–6545.

[28] M.-P. Egloff, H. Malet, Á. Putics, M. Heinonen, H. Dutartre, A. Frangeul, A. Gruez, V. Campanacci, C. Cambillau, J. Ziebuhr, Structural and functional basis for ADP-ribose and poly (ADP-ribose) binding by viral macro domains, J. Virol. 80 (2006) 8493–8502.
[29] C. Li, Y. Debing, G. Jankevicius, J. Neyts, I. Ahel, B. Coutard, B. Canard, Viral macro domains reverse protein ADP-ribosylation, J. Virol. 90 (2016) 8478–8486.
[30] M. Neuvonen, T. Ahola, Differential activities of cellular and viral macro domain proteins in binding of ADP-ribose metabolites, J. Mol. Biol. 385 (2009) 212–225.
[31] G. Shin, S.A. Yost, M.T. Miller, E.J. Elrod, A. Grakoui, J. Marcotrigiano, Structural and functional insights into alphavirus polyprotein processing and pathogenesis, Proc. Natl. Acad. Sci. U. S. A. 109 (2012) 16534–16539.
[32] M.D. Daugherty, J.M. Young, J.A. Kerns, H.S. Malik, Rapid evolution of PARP genes suggests a broad role for ADP-ribosylation in host–virus conflicts, PLoS Genet. 10 (2014), e1004403.
[33] J.G.M. Rack, D. Perina, I. Ahel, Macrodomains: structure, function, evolution, and catalytic activities, Annu. Rev. Biochem. 85 (2016) 431–454.
[34] S. Atasheva, M. Akhrymuk, E.I. Frolova, I. Frolov, New PARP gene with an anti-alphavirus function, J. Virol. 86 (2012) 8147–8160.
[35] L. Eckei, S. Krieg, M. Bütepage, A. Lehmann, A. Gross, B. Lippok, A.R. Grimm, B.M. Kümmerer, G. Rossetti, B. Lüscher, The conserved macrodomains of the non-structural proteins of Chikungunya virus and other pathogenic positive strand RNA viruses function as mono-ADP-ribosylhydrolases, Sci. Rep. 7 (2017), 41746.
[36] J.Y.-S. Leung, M.M.-L. Ng, J.J.H. Chu, Replication of alphaviruses: a review on the entry process of alphaviruses into cells, Adv. Virol. 2011 (2011).
[37] R. Abraham, D. Hauer, R.L. McPherson, A. Utt, I.T. Kirby, M.S. Cohen, A. Merits, A.K. Leung, D.E. Griffin, ADP-ribosyl-binding and hydrolase activities of the alphavirus nsP3 macrodomain are critical for initiation of virus replication, Proc. Natl. Acad. Sci. U. S. A. 115 (2018) E10457–E10466.
[38] R. Gupte, Z. Liu, W.L. Kraus, PARPs and ADP-ribosylation: recent advances linking molecular functions to biological outcomes, Genes Dev. 31 (2017) 101–126.
[39] F.R. Althaus, H. Hilz, S. Shall, ADP-Ribosylation of Proteins, Springer Verlag, Berlin, 2012.
[40] M.O. Hottiger, M. Boothby, F. Koch-Nolte, B. Lüscher, N.M. Martin, R. Plummer, Z.-Q. Wang, M. Ziegler, Progress in the function and regulation of ADP-ribosylation, Sci. Signal. 4 (2011) mr5.
[41] R. Sharifi, R. Morra, C.D. Appel, M. Tallis, B. Chioza, G. Jankevicius, M.A. Simpson, I. Matic, E. Ozkan, B. Golia, Deficiency of terminal ADP-ribose protein glycohydrolase TARG1/C6orf130 in neurodegenerative disease, EMBO J. 32 (2013) 1225–1237.
[42] B. Lüscher, M. Bütepage, L. Eckei, S. Krieg, P. Verheugd, B. H. Shilton, ADP-ribosylation, a multifaceted posttranslational modification involved in the control of cell physiology in health and disease, Chem. Rev. 118 (2017) 1092–1136.
[43] C. Liu, X. Yu, ADP-Ribosyltransferases and poly ADP-ribosylation, Curr. Protein Pept. Sci. 16 (2015) 491–501.
[44] P. Bai, Biology of poly (ADP-ribose) polymerases: the factotums of cell maintenance, Mol. Cell 58 (2015) 947–958.
[45] J. Morales, L. Li, F.J. Fattah, Y. Dong, E.A. Bey, M. Patel, J. Gao, D.A. Boothman, Review of poly (ADP-ribose) polymerase (PARP) mechanisms of action and rationale for targeting in cancer and other diseases, Crit. Rev. Eukaryot. Gene Expr. 24 (2014) 15–28.
[46] E. Melekis, A.C. Tsika, J. Lichière, C.T. Chasapis, I. Margiolaki, N. Papageorgiou, B. Coutard, D. Bentrop, G.A. Spyroulias, NMR study of non-structural proteins—part I: 1H, 13C, 15N backbone and side-chain resonance assignment of macro domain from Mayaro virus (MAYV), Biomol. NMR Assign. 9 (2015) 191–195.
[47] P. Güntert, C. Mumenthaler, K. Wüthrich, Torsion angle dynamics for NMR structure calculation with the new program Dyana, J. Mol. Biol. 273 (1997) 283–298.
[48] D. Pearlman, D. Case, J. Caldwell, W. Ross, T. Cheatham, D. Ferguson, G. Seibel, U. Singh, P. Weiner, P. Kollman, AMBER 5.0, University of California, San Francisco, 1997.
[49] L. Holm, L.M. Laakso, Dali server update, Nucleic Acids Res. 44 (2016) W351–W355.
[50] R. Zapata-Pérez, F. Gil-Ortiz, A.B. Martínez-Moñino, A.G. García-Saura, J. Juanhuix, Á. Sánchez-Ferrer, Structural and functional analysis of *Oceanobacillus iheyensis* macrodomain reveals a network of waters involved in substrate binding and catalysis, Open Biol. 7 (2017), 160327.
[51] R.L. McPherson, R. Abraham, E. Sreekumar, S.-E. Ong, S.-J. Cheng, V.K. Baxter, H.A. Kistemaker, D.V. Filippov, D. E. Griffin, A.K. Leung, ADP-ribosylhydrolase activity of Chikungunya virus macrodomain is critical for virus replication and virulence, Proc. Natl. Acad. Sci. U. S. A. 114 (2017) 1666–1671.
[52] J.J. Ziarek, F.C. Peterson, B.L. Lytle, B.F. Volkman, Binding site identification and structure determination of protein–ligand complexes by NMR, Methods Enzymol. 493 (2011) 241.
[53] M.V. Lykouras, A.C. Tsika, J. Lichière, N. Papageorgiou, B. Coutard, D. Bentrop, G.A. Spyroulias, NMR study of non-structural proteins—part III: 1 H, 13 C, 15 N backbone and side-chain resonance assignment of macro domain from Chikungunya virus (CHIKV), Biomol. NMR Assign. 12 (2018) 31–35.
[54] I.R. Kleckner, M.P. Foster, An introduction to NMR-based approaches for measuring protein dynamics, Biochim. Biophys. Acta 1814 (2011) 942–968.
[55] E.R. Zuiderweg, Mapping protein–protein interactions in solution by NMR spectroscopy, Biochemistry 41 (2002) 1–7.
[56] T. Haikarainen, L. Lehtiö, Proximal ADP-ribose hydrolysis in trypanosomatids is catalyzed by a macrodomain, Sci. Rep. 6 (2016), 24213.
[57] A.H. Forst, T. Karlberg, N. Herzog, A.-G. Thorsell, A. Gross, K.L. Feijs, P. Verheugd, P. Kursula, B. Nijmeijer, E. Kremmer, Recognition of mono-ADP-ribosylated ARTD10 substrates by ARTD8 macrodomains, Structure 21 (2013) 462–475.
[58] J.A. Wojdyla, I. Manolaridis, E.J. Snijder, A.E. Gorbalenya, B. Coutard, Y. Piotrowski, R. Hilgenfeld, P.A. Tucker, Structure of the X (ADRP) domain of nsp3 from feline coronavirus, Acta Crystallogr. D 65 (2009) 1292–1300.
[59] G. Timinszky, S. Till, P.O. Hassa, M. Hothorn, G. Kustatscher, B. Nijmeijer, J. Colombelli, M. Altmeyer, E.H. Stelzer, K. Scheffzek, A macrodomain-containing histone rearranges chromatin upon sensing PARP1 activation, Nat. Struct. Mol. Biol. 16 (2009) 923–929.
[60] M.A. Johnson, A. Chatterjee, B.W. Neuman, K. Wüthrich, SARS coronavirus unique domain: three-domain molecular architecture in solution and RNA binding, J. Mol. Biol. 400 (2010) 724–742.
[61] Y. Piotrowski, G. Hansen, A.L. Boomaars-van der Zanden, E.J. Snijder, A.E. Gorbalenya, R. Hilgenfeld, Crystal

structures of the X-domains of a Group-1 and a Group-3 coronavirus reveal that ADP-ribose-binding may not be a conserved property, Protein Sci. 18 (2009) 6–16.
[62] J. Lei, Y. Kusov, R. Hilgenfeld, Nsp3 of coronaviruses: structures and functions of a large multi-domain protein, Antivir. Res. 149 (2018) 58–74.
[63] C. Bartels, T.-h. Xia, M. Billeter, P. Güntert, K. Wüthrich, The program XEASY for computer-supported NMR spectral analysis of biological macromolecules, J. Biomol. NMR 6 (1995) 1–10.
[64] R. Keller, The Computer Aided Resonance Assignment Tutorial, Cantina Verlag, Goldau, Switzerland, 2004.
[65] Y. Shen, F. Delaglio, G. Cornilescu, A. Bax, TALOS+: a hybrid method for predicting protein backbone torsion angles from NMR chemical shifts, J. Biomol. NMR 44 (2009) 213–223.
[66] W. DeLano, The PyMOL Molecular Graphics System, Version 2.0, Schrödinger LLC, 2010.
[67] M.P. Williamson, Using chemical shift perturbation to characterise ligand binding, Prog. Nucl. Magn. Reson. Spectrosc. 73 (2013) 1–16.
[68] S. Lee, A.-R. Lee, K.-S. Ryu, J.-H. Lee, C.-J. Park, NMR investigation of the interaction between the RecQ C-terminal domain of human bloom syndrome protein and G-quadruplex DNA from the human c-Myc promoter, J. Mol. Biol. 431 (2019) 794–806.
[69] J. Xu, A.V. Sarma, Y. Wei, L.J. Beamer, S.R. Van Doren, Multiple ligand-bound states of a Phosphohexomutase revealed by principal component analysis of NMR peak shifts, Sci. Rep. 7 (2017) 5343.
[70] H. Qi, F.o.-X. Cantrelle, H. Benhelli-Mokrani, C. Smet-Nocca, L. Buée, G. Lippens, E. Bonnefoy, M.-C. Galas, I. Landrieu, Nuclear magnetic resonance spectroscopy characterization of interaction of Tau with DNA and its regulation by phosphorylation, Biochemistry 54 (2015) 1525–1533.
[71] P. Contursi, B. Farina, L. Pirone, S. Fusco, L. Russo, S. Bartolucci, R. Fattorusso, E. Pedone, Structural and functional studies of Stf76 from the Sulfolobus islandicus plasmid–virus pSSVx: a novel peculiar member of the winged helix–turn–helix transcription factor family, Nucleic Acids Res. 42 (2014) 5993–6011.